Enhanced efficiency of organic light-emitting devices by employing a periodically corrugated conductive photoresist

2015 Appl. Phys. Express 8 022102

(http://iopscience.iop.org/1882-0786/8/2/022102)

Applied Physics Express **8**, 022102 (2015)
http://dx.doi.org/**10.7567/APEX.8.022102**

Enhanced efficiency of organic light-emitting devices by employing a periodically corrugated conductive photoresist

Yu Bai, Yi Fan, Qipeng Lu, Xiaoyi Wang, Minghui Chu, and Xingyuan Liu*

State Key Laboratory of Luminescence and Applications, Changchun Institute of Optics, Fine Mechanics and Physics, Chinese Academy of Sciences, Changchun 130033, China
E-mail: liuxy@ciomp.ac.cn

Received November 4, 2014; accepted December 14, 2014; published online January 8, 2015

Photons trapped in the form of waveguide (WG) modes associated with the organic/organic interface and in the form of surface plasmon polariton (SPP) modes associated with the metallic electrode/organic interface result in a large energy loss in organic light-emitting devices (OLEDs). We demonstrate the efficient outcoupling of WG and SPP modes by integrating a wavelength-scale periodically corrugated conductive photoresist into the device structure. The corrugated OLEDs with appropriate grating periods lead to a 15.9% increase in efficiency compared with the planar OLEDs. The efficient outcoupling of the WG and SPP modes is verified by the numerical simulation of both the emission spectra and the field distribution. © 2015 The Japan Society of Applied Physics

It is well known that light extraction is one of the bottlenecks to achieve high efficiency in light-emitting diodes (LEDs) and organic light-emitting devices (OLEDs). For OLED structures, around 80% of internal generated light is trapped in the form of waveguide (WG) modes in organic and indium–tin oxide (ITO) anode layers, and in the form of SPP modes associated with the metallic cathode/organic interface.[1,2] The power lost even reaches 95% for the inorganic LEDs owing to the high refractive index of inorganic semiconductors.[3,4] To enhance light extraction, microstructures have been introduced into LED devices by various lithography-based technologies, which are suitable to inorganic semiconductors owing to their high physical and chemical stabilities. However, these approaches are difficult to apply to OLEDs because organic materials are generally soluble in the solvents used in conventional lithography, and the OLEDs would deteriorate optically or electrically when exposed to water, oxygen, or high-energy electrons.

In order to avoid the degradation of OLEDs, microstructure processing has to start from the substrate, so that the corrugation proceeds from the organic layer to the opposite electrode. Periodic corrugations on silica substrates induced by holographic lithography first and then by reactive ion etching (RIE), and a spontaneously formed quasi-periodic structure on a glass substrate have been reported.[5–9] Although the trapped optical modes were found coupled out from microstructured OLEDs produced by these means, the substrate pattern transmission approach faces the problem of electric field distortion due to the uneven ITO surface. The device endurance to high voltages therefore worsens and they are subjected to a higher probability of breakdown. It is obvious that the problem can be solved if microstructures are introduced into an organic functional layer without affecting the flatness of the ITO electrode film. Efforts have been paid along this line, for instance, micromolding dendrimers above the ITO anode.[10,11] However, the practical application of the technology is restricted because of the complexity of the fabrication process and the high fluidity requirement of the polymer.[12,13] Recently, it has been reported that a periodic corrugation structure obtained by laser ablation in an organic layer could increase the OLED efficiency.[14] However, laser ablation may affect the electrical properties of the organic thin film and limit the selection of materials. In this study, a dual-beam laser interference exposure method is developed to induce periodic corrugation in the organic hole injection layer (HIL) with a conductive photoresist. Increases in luminance and efficiency are observed in OLEDs with a wavelength-scale periodic corrugation.

An ITO-coated glass substrate was cleaned with acetone and ethanol. The conductive photoresist was obtained by the incorporation of a conductive polymer, poly(3,4-ethylene dioxythiophene)–poly(styrene sulfonic acid) (PEDOT:PSS) with a concentration of 1.3–1.7 wt % in an aqueous solution, into a normal photoresist S1805 (Rohm and Haas). First, PEDOT:PSS aqueous solution and alcohol were mixed at a volume ratio of 1 : 1 (hereafter referred to as P). Then, photoresist S1805 and acetone were mixed at a volume ratio of 1 : 1 (hereafter referred to as S). Lastly, the conductive photoresist was obtained by mixing S and P at different volume ratios. The HIL was spin-coated at 3000 rpm to obtain a 200 nm thickness. The sample was prebaked on a hot plate in air for 1 min at 95 °C. Then, the sample was exposed to two beams that were split from the 457 nm CW laser with a beam diameter of 2 mm. The microstructure fabrication was conducted in air at room temperature. The morphologies of the microstructure were characterized by atomic force microscopy (AFM; Shimadzu SPM-9700) in the phase mode. The ITO substrates coated with the corrugated HIL were immediately transferred to a thermal evaporation chamber. The 60-nm-thick hole-transporting layer (HTL) of *N*,*N*′-diphenyl-*N*,*N*′-bis(1,1′-biphenyl)-4,4′-diamine (NPB), the 70-nm-thick emitting layer (EML) of tris(8-hydroxyquinoline) aluminum (Alq_3), and the cathode of LiF (1 nm)/Al (100 nm) were evaporated sequentially. To investigate the effect of the grating, planar OLEDs were fabricated in the flat region of the ITO glass substrate. Here, all layers were prepared by thermal evaporation in a high vacuum of less than 5×10^{-4} Pa. The active area of the devices was 1×1 mm^2. The current density–voltage–luminance (*J*–*V*–*L*) characteristics were measured using a Keithley 2611 digital source meter and a Konica Minolta CS-100A luminance meter. The electroluminescent (EL) emission spectra were recorded using an Ocean Optics fiber spectrometer. All of the measurements were conducted in air at room temperature.

The WG and SPP resonances at the corrugated metal surface were tuned by adjusting the grating period. Their overlap with the emitting spectra of OLEDs is crucial for

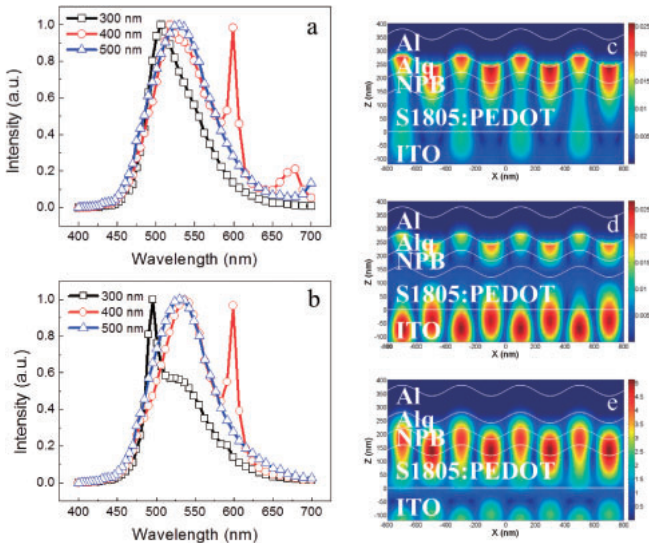

Fig. 1. Calculated EL emission spectra in TM (a) and TE (b) modes under various corrugation periods in the normal direction. FDTD simulated distribution of magnetic field intensity in the microstructured OLEDs with 400 nm period at the incident polarized light wavelengths of 679 (c) and 599 nm (d) in TM mode, and 598 nm (e) in TE mode. Here, x is the coordinate along the direction of periodic corrugation and z is the coordinate along the direction of thickness of the device.

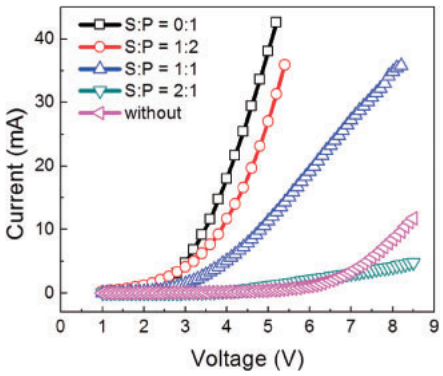

Fig. 2. Voltage–current characteristics of the hole-only devices with different volume doping concentrations of conductive photoresist.

improving the light extraction efficiency of OLEDs. First, a theoretical simulation of EL spectra in the normal direction was performed for OLEDs with grating periods ranging from 300 to 500 nm to determine the desired grating period. In-house-generated finite-difference time-domain (FDTD) codes were applied to simulate the emission spectra. For simulation, several point light sources, the emission spectra of which originate from the Alq_3 EL spectrum, were put in the emission layer in different positions and polarization directions. The simulated EL spectra were obtained from the output spectra of the devices. The simulated EL spectra of the corrugated device with various periods are shown in Figs. 1(a) [transverse magnetic (TM) mode] and 1(b) [transverse electric (TE) mode]. Several extra emission maxima are observed to exhibit a blue shift with decreasing grating period [Figs. 1(a) and 1(b)]. The effective improvement of extra emission peaks in the TM and TE modes for the 400 nm corrugated device suggests that 400 nm is a favorable grating period. In order to identify the two emission maxima and establish the optical modes supported by the corrugated OLEDs, the spatial steady-state Hz field intensity distribution of the TM and TE modes across the device structure as a function of position with the normal incident light was calculated for the device with a 400 nm grating period. Figures 1(c)–1(e) show the field distributions in the normal direction at three peak EL wavelengths of 679, 599, and 598 nm, respectively. The field intensity is maximum at the Al/Alq_3 interface and decays along the direction perpendicular to the interface at the wavelength of 679 nm [Fig. 1(c)]. We can conclude that the field distribution at the 679 nm emission wavelength originates from the SPP mode, since SPPs are surface waves and propagate along the interface between a metal and a dielectric.[15–19] On the other hand, the fields at the wavelengths of 599 and 598 nm are mainly confined within the ITO and organic layers [Figs. 1(d)–1(e)], which should be assigned to the TM and TE polarized WG modes owing to the high refractive indices of the ITO and organic layers. Therefore, the additional peaks shown in the simulated EL spectra in Figs. 1(a) and 1(b) are identified as the SPP mode associated with the Al cathode/organic interface and the WG mode confined within the ITO and organic layers, respectively.

The dual-beam laser interference exposure method was used to induce periodic corrugation on the conductive photoresist after determining the grating period. In the conductive photoresist, S1805 is not conductive. PEDOT:PSS was doped into S1805 to enhance the hole injection and transport of the HIL. In order to verify the conductivity of the HIL at different volume doping concentrations, the hole-only device with the structure of ITO/S:P/NPB (30 nm)/Al (100 nm) was fabricated. To investigate the hole injection effect of the HIL, a hole-only device without the conductive photoresist was fabricated. The device structure is ITO/NPB (30 nm)/Al (100 nm). The voltage–current density characteristics show that the conductivity of the conductive photoresist increases with the doping concentration of PEDOT:PSS (Fig. 2). This is reasonable since S1805 is not conductive, and the conductivity of the conductive photoresist is completely due to PEDOT:PSS. At low voltages, the conductivity of the hole-only device with the conductive photoresist is even higher than that of the device without the conductive photoresist. This is due to the fact that PEDOT:PSS has a more suitable highest occupied molecular orbital level than NPB, resulting in a better hole injection from ITO. The current density of the device ($S : P = 2 : 1$) gradually becomes lower than that of the device without the conductive photoresist at around 7 V owing to the inferior conductivity of the low PEDOT:PSS doping concentration. For the high PEDOT:PSS doping concentration, owing to its high conductivity, the current density is still larger than that of the device without the conductive photoresist. However, a high doping concentration of PEDOT:PSS would affect the light photolysis reaction of S1805 and lead to an unsuitable grating structure. The morphologies of the corrugated structure on the conductive photoresist surface were characterized by AFM [Figs. 3(a) and 3(b)], in which the doping concentrations of $S : P$ are $1 : 1$ and $2 : 1$, respectively. The depth of corrugation is about 40 nm. As described above, periodic corrugation could not be induced by using the high doping concentration of PEDOT:PSS. Therefore, considering the

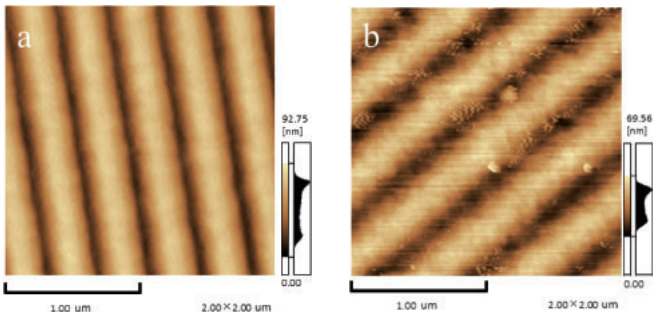

Fig. 3. AFM image of surface morphologies of corrugated photoresist, with the doping concentrations of the conductive photoresist of S : P = 1 : 1 (a) and 2 : 1 (b).

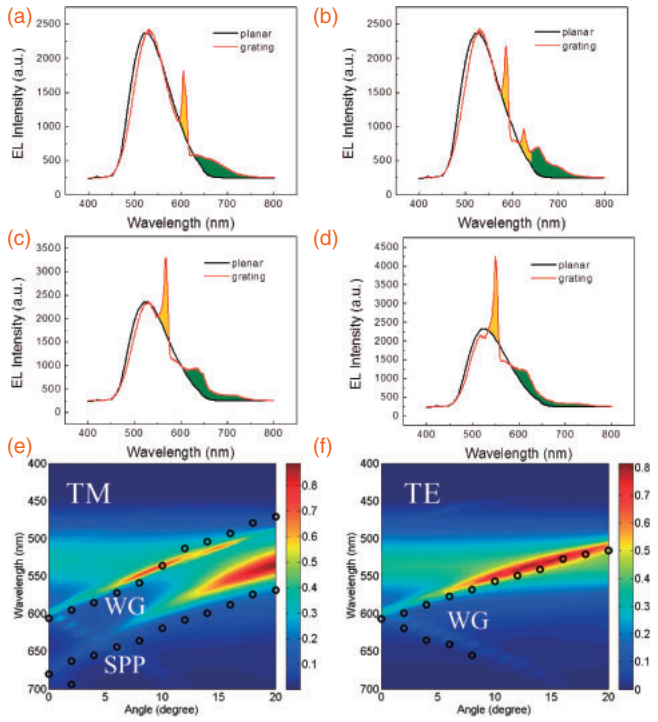

Fig. 4. Measured EL spectra for the planar and 400 nm grating devices with different detection angles of 0 (a), 4 (b), 8 (c), and 12° (d). Yellow and green colors roughly show the portions from the WG and SPP modes. Measured (circle) and simulated TM (e) and TE (f) polarization dispersion relations of the corrugated OLEDs. The color bar means the normalized intensity of the simulated spectra.

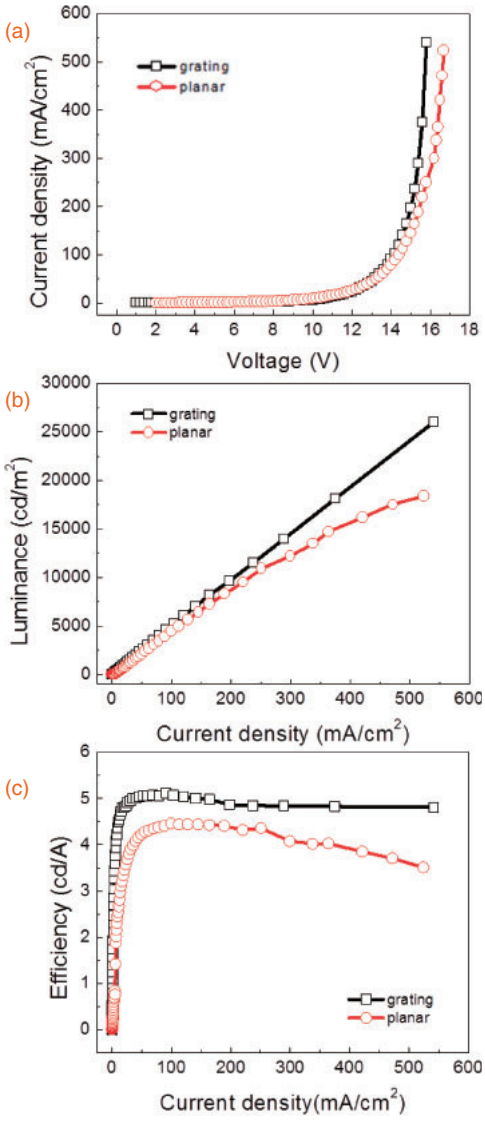

Fig. 5. Voltage–current density (a), luminance–current density (b), and efficiency–current density (c) characteristics of the corrugated and planar OLEDs.

conductivity and morphology factors, we choose a moderate doping concentration of S : P (1 : 1) for the induction of periodic corrugation in the HIL.

The EL spectra for both planar and grating devices were measured at 100 mA/cm^2 with angles of 0, 4, 8, and 12° [Figs. 4(a)–4(d), respectively]. The peak emission at 599 nm (yellow) results from an efficient light outcoupling of the trapped WG modes, and that at 679 nm (green) from the outcoupling of the trapped SPP modes [Fig. 4(a)]. With the increase in detection angle, splitting phenomena can be observed in emissions from the WG and SPP modes, such as two emission peaks at 570 and 610 nm from WG modes, and two emission peaks at 655 and 705 nm from SPP modes at the detection angle of 4° [Fig. 4(b)]. The dispersion map derived from the simulated EL spectra of the corrugated device for both TM and TE polarizations shows that the EL intensity appears as a function of both viewing angle and EL wavelength [Figs. 4(e) and 4(f)]. The dispersion relation curve constructed from the experimental EL emission spectra with both TM and TE polarizations shows good consistency with the theoretical calculation ones. The optical modes within the device structure that appear as EL maxima indicate an efficient outcoupling of light from those optical modes, which are normally nonradiative, by the addition of the appropriate wavelength-scale microstructure.

The EL performance characteristics of the Alq_3-based OLEDs with and without the corrugated structure are shown in Figs. 5(a)–5(c). The OLEDs show comparable current densities at the same driving voltage, as shown in Fig. 5(a). The curves were obtained by averaging several measurements. Compared with that of the planar OLEDs, the EL performance of the corrugated OLED with a 400 nm grating period was notably enhanced by increasing the maximum luminance from 18400 to 26000 cd/m^2, and a 15.9% enhancement in maximum current efficiency from 4.4 to 5.1 cd/A was obtained. This enhancement in EL efficiency confirms the above experimental and simulated results

indicating that the power lost to the WG and the SPP modes at the cathode/organic interface is recovered as a useful light emission, which contributes to the much enhanced light extraction.[1)] The fraction of the power trapped in WG and SPPs depends on device structural properties, for example, the refractive index and layer thickness of the materials employed in the devices.[20,21)] In our case, a number of photons trapped in WG and SPPs may not be extracted. It is possible to further improve light extraction by tuning the parameters of the microstructure and device structure to shift both WG and SPP modes close to the peak wavelength of Alq_3 and enhance the coupling efficiency between the optical modes and the electroluminescence. For example, employing a two-dimensional (2D) microstructure is another potential approach to further improve light extraction, owing to its higher efficiency in coupling SPPs to far-field radiation.[22)]

In summary, a conductive photoresist is developed for the preparation of periodically corrugated microstructures in an organic layer of OLEDs by a dual-beam laser interference exposure method. A wavelength-scale periodically corrugated structure with the conductive photoresist allows the outcoupling of the WG and SPP modes associated with the cathode/organic interface, which are usually trapped within normal planar devices, and results in a 15.9% enhancement in EL efficiency. Our results demonstrate that the efficient periodically corrugated structure can be easily introduced into an organic functional layer by the conductive photoresist in OLEDs and that the power lost to the WG and SPP modes can be recovered, thus opening an avenue to enhance the OLED efficiency.

Acknowledgments This work is supported by the CAS Innovation Program, the National Science Foundation of China (No. 51102228), and a project supported by State Key Laboratory of Luminescence and Applications.

1) P. A. Hobson, S. Wedge, J. A. E. Wasey, I. Sage, and W. L. Barnes, Adv. Mater. **14**, 1393 (2002).
2) G. Gu, D. Z. Garbuzov, P. E. Burrows, S. Venkatesh, and S. R. Forrest, Opt. Lett. **22**, 396 (1997).
3) D. H. Kim, C. O. Cho, Y. G. Roh, H. Jeon, Y. S. Park, J. Cho, J. S. Im, C. Sone, Y. Park, W. J. Choi, and Q. H. Park, Appl. Phys. Lett. **87**, 203508 (2005).
4) A. A. Erchak, D. J. Ripin, S. Fan, P. Rakich, J. D. Joannopoulos, E. P. Ippen, G. S. Petrich, and L. A. Kolodziejski, Appl. Phys. Lett. **78**, 563 (2001).
5) J. Feng, T. Okamoto, and S. Kawata, Opt. Lett. **30**, 2302 (2005).
6) K. Hong, H. K. Yu, I. Lee, K. Kim, S. Kim, and J. L. Lee, Adv. Mater. **22**, 4890 (2010).
7) W. H. Koo, S. M. Jeong, F. Araoka, K. Ishikawa, S. Nishimura, T. Toyooka, and H. Takezoe, Nat. Photonics **4**, 222 (2010).
8) Y. G. Bi, J. Feng, Y. F. Li, Y. Jin, Y. F. Liu, Q. D. Chen, and H. B. Sun, Appl. Phys. Lett. **100**, 053304 (2012).
9) Y. Jin, J. Feng, X. L. Zhang, Y. G. Bi, Y. Bai, L. Chen, T. Lan, Y. F. Liu, Q. D. Chen, and H. B. Sun, Adv. Mater. **24**, 1187 (2012).
10) E. King, Y. Xia, X.-M. Zhao, and G. M. Whitesides, Adv. Mater. **9**, 651 (1997).
11) J. R. Lawrence, G. A. Turnbull, and I. D. W. Samuel, Appl. Phys. Lett. **82**, 4023 (2003).
12) C. J. Yates, I. D. W. Samuel, P. L. Burn, S. Wedge, and W. L. Barnes, Appl. Phys. Lett. **88**, 161105 (2006).
13) J. Wang, X. Sun, L. Chen, and S. Y. Chou, Appl. Phys. Lett. **75**, 2767 (1999).
14) Y. Bai, J. Feng, Y. F. Liu, J. F. Song, J. Simonen, Y. Jin, Q. D. Chen, J. Zi, and H. B. Sun, Org. Electron. **12**, 1927 (2011).
15) W. L. Barnes, A. Dereux, and T. W. Ebbesen, Nature **424**, 824 (2003).
16) D. van Oosten, M. Spasenović, and L. Kuipers, Nano Lett. **10**, 286 (2010).
17) H. Gao, J. Henzie, and T. W. Odom, Nano Lett. **6**, 2104 (2006).
18) W. C. Liu and D. P. Tsai, Phys. Rev. B **65**, 155423 (2002).
19) J. Li and C. Z. Ning, Phys. Rev. Lett. **93**, 087402 (2004).
20) D. M. Koller, A. Hohenau, H. Ditlbacher, N. Galler, F. R. Aussenegg, A. Leitner, J. R. Krenn, S. Eder, S. Sax, and J. W. List, Appl. Phys. Lett. **92**, 103304 (2008).
21) S. Nowy, B. C. Krummacher, J. Frischeisen, N. A. Reinke, and W. Brütting, J. Appl. Phys. **104**, 123109 (2008).
22) P. T. Worthing and W. L. Barnes, Appl. Phys. Lett. **79**, 3035 (2001).